Anisotropic Electron Tail Generation during Tearing Mode Magnetic Reconnection

Ami M. DuBois, Abdulgader F. Almagri, Jay K. Anderson, Daniel J. Den Hartog, John David Lee, and John S. Sarff

Phys. Rev. Lett. **118**, 075001 — Published 14 February 2017

DOI: 10.1103/PhysRevLett.118.075001

Anisotropic electron tail generation during tearing mode magnetic reconnection

Ami M. DuBois*, Abdulgader F. Almagri, Jay K. Anderson, Daniel J. Den Hartog, John David. Lee, John S. Sarff

Department of Physics, University of Wisconsin – Madison, Madison, WI, 53706, USA

The first experimental evidence of anisotropic electron energization during magnetic reconnection that favors a direction perpendicular to the guide magnetic field in a toroidal, magnetically confined plasma is reported in this Letter. Magnetic reconnection plays an important role in particle heating, energization, and transport in space and laboratory plasmas. In toroidal devices like the Madison Symmetric Torus, discrete magnetic reconnection events release large amounts of energy from the equilibrium magnetic field. Fast x-ray measurements imply a non-Maxwellian, anisotropic energetic electron tail is formed at the time of reconnection. The tail is well described by a power-law energy dependence. The expected bremsstrahlung from an electron distribution with an anisotropic energetic tail ($v_\perp > v_\parallel$) spatially localized in the core region is consistent with x-ray emission measurements. A turbulent process related to tearing fluctuations is the most likely cause for the energetic electron tail formation.

Magnetic reconnection (MR) is characterized by impulsive, discrete bursts of released magnetic energy (U_{mag}). The release of U_{mag} and conversion to kinetic energy, plays an important role in particle transport and energization (heating and acceleration) in space and laboratory plasmas. In particular, electron energization during MR has been observed in the magnetotail[1–3], during magnetospheric substorms[4,5], during solar flares[6,7], and in laboratory experiments[8–15]. However, the mechanisms leading to the onset of MR and the energization of particles are not fully understood.

One of the major outstanding questions for electron acceleration during MR is whether the process is localized inside or outside of the diffusion region. The WIND spacecraft provided the first evidence of electron acceleration localized to the diffusion region, where the power-law spectra were more energetic compared to the outflow region and favors directions parallel/anti-parallel to the guide field.[3] The symmetry between the parallel/anti-parallel spectra suggests electrons may be energized by a process other than parallel electric fields in the diffusion region. It was later confirmed by CLUSTER that electrons can be accelerated by pitch angle scattering.[16] Relative to space-based observations, where *in-situ* measurements are challenging, laboratory experiments provide a controlled environment to study electron energization during MR. Electron energization is commonly observed during the internal kink mode sawtooth cycle in tokamak plasmas. Parallel/anti-parallel anisotropy in x-ray emission from non-thermal electrons, attributed to runaway acceleration driven by the inductive electric field created during the impulsive sawtooth crash, has been measured in the T-10[10], VTF[8], TCV[9], and PLT[11] tokamaks.

This Letter presents the first experimental evidence for anisotropic electron energization during MR that favors a direction perpendicular to the mean (or guide) magnetic field in a toroidal, magnetically confined plasma. The anisotropy appears as a non-thermal tail in the x-ray energy spectrum during MR events in reversed field pinch (RFP) plasmas. The x-ray tail fits a power-law that flattens during MR. Runaway energization is ruled out by measured parallel/anti-parallel symmetry in the x-ray flux. This is also the first evidence that electron energization accompanies the better-studied ion energization during MR in RFP plasmas[17,18].

The experiments described below were performed in the MST[19] RFP experiment having a major radius R=1.5m and a minor radius a=0.52m. MR in RFP plasmas stems from several tearing modes that are destabilized by the parallel current density gradient, and the nonlinear interaction between stable and unstable modes results in a quasi-periodic magnetic relaxation cycle that causes a sudden release of stored U_{mag} during the fast (~100μs) crash phase.[20] This cycle resembles the internal kink mode sawtooth process in tokamak plasmas in some respects, but it is more global in RFP plasmas due to its multi-mode nature. The overlap of magnetic islands from multiple tearing modes leads to widespread magnetic stochasticity, enhancing particle and energy transport.[21–23] Fig. 1 shows two typical magnetic relaxation cycles during a single discharge in MST. Fig. 1a shows U_{mag} during a 10ms window. The magnetic fluctuation amplitudes for an unstable core-resonant m=1, n=6 mode (blue,

dashed) and a nonlinearly-driven edge-resonant m=0, n=1 mode (red, solid) are shown in Fig. 1b, where m and n are the poloidal and toroidal mode numbers. The insets in Fig. 1 show the evolution (relative to MR) of U_{mag} (top) and magnetic fluctuation amplitudes (bottom) averaged over 485 MR events. At the MR event, 20-30kJ of U_{mag} is released in 100μs, and both core and edge-resonant mode amplitudes peak.

While ions are strongly energized during MR events (bulk heating and energetic ion tail formation)[17,18], the thermal population of electrons are measured by Thomson scattering to cool following MR[23,24]. Magnetic stochasticity is maximum during MR, and high mobility makes electrons susceptible to rapid transport. Hence, possible energization of electrons is anticipated to be transient on a ~10μs timescale, making high time resolution measurements necessary to reveal electron dynamics. We report energy-resolved bremsstrahlung emission showing an enhancement in the high energy x-ray flux during MR events in MST plasmas. Measurements were taken with a fast x-ray (FXR) diagnostic[25] that consists of a Si avalanche photodiode with optimal energy range of 3–25keV and a 20ns Gaussian shaping time.

We first describe x-ray bremsstrahlung emission measured through a 150μm thick beryllium (Be) window with a line-of-sight along a minor radial chord with angular acceptance ~15° (Fig. 2, blue), intersecting the magnetic axis (called the radial view hereafter). Data were collected for plasmas with electron density n_e=0.8×10^{19}m^{-3} and plasma current I_p=500kA ($\langle B\rangle \sim 3\ kG$). The electron temperature in the core is $T_e(0)$~500eV. Fig. 3 shows the energy-resolved x-ray flux versus time relative to the MR event (t=0ms) for an ensemble of 485 MR events like those in Fig. 1, where black represents no measurable flux and red signifies high flux. The x-ray flux for E>20keV increases around t=0, indicating that energetic electrons are generated during MR. After the MR event, the high energy x-ray flux decays rapidly, implying the energetic electrons are quickly lost, consistent with expectations for stochastic transport.

To quantify the extent of energization, the x-ray distribution is averaged in 20μs windows around the MR event between 5 and 25keV. Fig. 4 shows x-ray spectra for 0.5ms before (black), during (red), and 0.5ms after (blue) MR. The error bars in Fig. 4 (and Fig. 6 below) are calculated from the uncertainty in the number of x-ray counts, $\sqrt{n}$ (standard deviation for Poisson distributions). To model the flux (Γ) as a function of energy, each spectrum is fit with a power-law, $\Gamma(E) \propto E^{-\gamma}$, where γ is the tail spectral index. The smaller the γ, the greater the number of energetic x-rays are generated and the flatter the tail becomes. The error in γ (hereafter) is estimated from the variance-covariance matrix of the least squares power-law fit for each spectrum. For the spectra in Fig. 4, γ in the radial view ($\gamma_\perp$) decreases from 4.15 ± 0.03 to 2.15 ± 0.05 during MR, indicating significant flattening of the high energy tail. After the MR event, $\gamma_\perp$ increases to 6.77 ± 0.09, indicating the non-thermal electrons are lost from the plasma. The inset of Fig. 4 shows $\gamma_\perp$ in 20μs intervals. Before the MR event, $\gamma_\perp$ is

constant, but decreases when the U_{mag} begins decreasing (t~-70μs). In as little as 60μs, $\gamma_\perp$ reaches a minimum before there is a loss in high energy x-ray flux.

In principle, runaway acceleration of electrons due to the inductive electric field parallel to **B** could produce an energetic x-ray tail in MST plasmas. Experiments in the PLT tokamak studying the angular distribution of bremsstrahlung emitted from runaway electrons showed that x-ray emission peaks in the direction in which electrons travel, leading to a measured toroidal anisotropy in the x-ray velocity distribution.[11] Modeling of the bremsstrahlung angular distribution shows this anisotropy occurs for electron energies as low as 10s of keV.[26] If the observed electron energization in MST plasmas is associated with runaway acceleration, the x-ray emission should peak in the direction of the parallel electric field, leading to an anisotropic bremsstrahlung angular distribution. To simulate the expected x-ray flux for electron runaway, we use the CQL3D code (a relativistic collisional/quasilinear 3D Fokker-Planck solver[27]) to model a stationary test electron distribution with a mock runaway tail having a power-law energy distribution localized in $v_{||}$ with density ~1% of a background thermal (500eV) Maxwellian distribution (Fig. 5a). The mock tail has a Gaussian radial profile centered on the magnetic axis with a 9cm radial extent. The code includes a calculation of x-ray bremsstrahlung along prescribed pencil-like lines-of-sight through the toroidal plasma volume, like that shown in Fig. 2. Fig. 5b shows the modeled x-ray spectra for toroidal lines-of-sight on the mid-plane tangential to the magnetic axis that view on-coming (parallel, black) and receding (anti-parallel, red) tail electrons. A radial (blue) line-of-sight through the magnetic axis is also shown. The x-ray flux in the toroidal views favors the parallel direction, as expected.[11]

To look for asymmetry in the x-ray flux in MST plasmas, the FXR detector was moved to a toroidal view port with a 150μm thick Be window and an acceptance angle of ~5° (Fig. 2, black) located just below mid-plane and centered on the magnetic axis. Experiments were performed with $E_\parallel$ in the normal (parallel) and reversed (anti-parallel) directions to assess asymmetry in the x-ray flux and underlying electron distribution function (EDF). Fig. 6 shows the x-ray spectra for a 20μs window during MR for views in the parallel (black), anti-parallel (red), and radial (blue) directions. The x-ray spectra measured in the toroidal views show tail formation, but they are parallel/anti-parallel symmetric within measurement uncertainty, with $\gamma_\parallel = 3.92 \pm 0.12$ and $\gamma_{anti-\parallel} = 3.73 \pm 0.14$. Hence, runaway acceleration is not consistent with the measured x-ray tail created by MR. Note that the toroidal views are not strictly parallel to **B** along the line-of-sight, but "||" is used for simplicity. For these plasmas, runaway generation is not expected to be strong since the net emf acting on electrons is below the critical (Dreicer[28]) field, $E_D = \frac{n_e e^3 \ln\Lambda}{4\pi\epsilon_0^2 m_e V_{the}^2}$. The net large-scale (magnetic flux-surface-average) emf from all contributions in Ohm's law must be balanced by $\eta J_\parallel$, where η is the Spitzer resistivity and $J_\parallel$ is the flux-surface-averaged parallel current density, both well known[23,29]. For these plasmas, $\eta J_\parallel / E_D \approx 0.12$. The electron tail contribution to $J_\parallel$ is < 20%.[30]

In addition to toroidal symmetry, measurements show higher x-ray flux (and a more substantial high energy tail) in the radial view than in the toroidal views for E>10keV during MR. This is also contrary to an EDF that has parallel anisotropy as indicated by the modeling above, which predicts the x-ray flux in the radial view to be an order of magnitude less than the toroidal views (Fig. 5b). The evolution of the experimentally observed $\gamma_\perp$ (blue) and $\gamma_\parallel$ (black) are shown in the inset of Fig. 6. To quantify tail generation, $\Delta\gamma = \gamma_{before} - \gamma_{during}$ is calculated before and during MR, with larger $\Delta\gamma$ indicating a larger tail. The $\Delta\gamma$ in the radial view ($\Delta\gamma_\perp = 2.17 \pm 0.02$) is almost twice as large as in the toroidal view ($\Delta\gamma_\parallel = 1.21 \pm 0.02$). Also, note that the tail generation occurs in a narrower time window for toroidal views than for the radial view, indicated by the width of γ around 0ms. The full-width-half-maximum of $\gamma_\perp$ is 65.9±3.3μs compared to 39.1±1.6μs for $\gamma_\parallel$. Also, the decrease in $\gamma_\parallel$ is delayed relative to $\gamma_\perp$, and $\gamma_\parallel$ relaxes faster than $\gamma_\perp$ following MR, suggesting an energization process that favors the perpendicular direction, with pitch angle scattering into the parallel direction, followed by relatively rapid parallel transport. Previous ion energization measurements in MST also show anisotropy favoring a perpendicular heating mechanism.[18] The strong correlation with tearing dynamics suggests a turbulent mechanism is similarly active for electron tail energization, although the precise mechanism could be different for electrons and ions.

To assess anisotropy favoring the perpendicular direction while maintaining toroidal symmetry, we model a stationary test EDF with an energetic tail having a power-law energy distribution localized in $v_\perp$, again with a density of 1% the background 500eV Maxwellian distribution (Fig. 5c). The Maxwellian EDF fills the whole plasma volume, but the radial profile of the tail is Gaussian, centered on the magnetic axis with a 9cm radial extent. Fig. 5d shows the predicted x-ray spectra for pencil-like lines-of-sight in the parallel (black), anti-parallel (red), and radial (blue) views. The predicted spectra in the toroidal views are symmetric, and for E>10keV, the flux is larger in the radial view. Thus, an electron tail distribution with strong perpendicular anisotropy is consistent with measurements of bremsstrahlung emission during MR in MST plasmas. Broadening the radial extent of the core-localized tail in the test EDF causes the predicted x-ray flux in toroidal views to eventually become larger than in the radial view, while narrowing the radial extent increases the x-ray flux in the radial view further. This implies that the fast electrons in MST plasmas must be radially localized to ~9cm of the magnetic axis. This might result in part from weaker stochastic transport in that region, e.g., the residual magnetic island structure associated with the innermost-resonant tearing mode might preserve the integrity of magnetic surfaces near the magnetic axis.

The electron tail correlates with the released U_{mag} during MR events. The stored U_{mag} within the plasma volume scales as U_{mag}~I_p^2, and the size of the MR event tends to be larger with lower n_e. X-ray measurements were obtained for a variety of plasmas with I_p=300-500kA and n_e=0.4-1.5×10^{19}m^{-3}. The U_{mag} released during MR, ΔU_{mag}, is easily determined using reconstructions of the magnetic equilibrium.[29] During MR, $\Delta\gamma_\perp$ increases from $\Delta\gamma_\perp$=1.94 for ΔU_{mag}~15kJ to $\Delta\gamma_\perp$=2.73 for ΔU_{mag}~55kJ. The strength of ion energization exhibits a similar trend

with ΔU_{mag}. The operation with $q(a)=0$ mutes ΔU_{mag} and electron (and ion) energization, since resonant $m=0$ modes that strongly couple to $m=1$ modes are removed from the plasma.

In summary, high-time-resolution measurements of x-ray energy spectra provide the first evidence of the formation of an anisotropic energetic electron tail in a toroidal plasma during MR that is not attributable to runaway acceleration. The bremsstrahlung photon energies extend to 20-30keV during tearing-driven MR in MST plasmas. The energetic tail is characterized by a power-law with a spectral index, which decreases from 4.15 to 2.15 during MR and rapidly increases following the event, consistent with stochastic transport expectations. The measured x-ray tail spectra are large in a radial view and parallel/anti-parallel symmetric in toroidal views, which rules out runaway acceleration as the responsible mechanism. An anisotropic EDF with a population of fast electrons localized in $v_\perp$ and spatially limited to the core region is consistent with the measured x-ray energy spectra. The dynamics of the x-ray tail correlate with the dynamics of tearing modes and the magnitude of U_{mag} released by MR, implying a turbulent process is the most likely cause for the anisotropic energetic electron tail formation. These results provide laboratory plasma evidence for electron energization due to a process other than parallel electric fields during MR, similar to WIND spacecraft observations. Perpendicular energization is also observed for ions in MST, which suggests similar mechanisms may operate simultaneously on electrons and ions. These results also provide new opportunity to better understand the conversion of U_{mag} and particle dynamics, to improve theories that accurately describe MR and particle energization, and to strengthen the connections between MR processes observed in space and laboratory experiments.

The authors thank the UW-Madison MST group for the many valuable discussions. This material is based upon work supported by the U.S. Department of Energy Office of Science, Office of Fusion Energy Sciences program under Award Number DE-FC02-05ER54814 and the National Science Foundation under Grant Number PHY08-21899.

[1] M. Hoshino, T. Mukai, T. Terasawa, and I. Shinohara, J. Geophys. Res. **106**, 25979 (2001).
[2] M. Hoshino, K. Hiraide, and T. Mukai, Earth, Planets Sp. **53**, 627 (2001).
[3] M. Øieroset, R.P. Lin, T.D. Phan, D.E. Larson, and S.D. Bale, Phys. Rev. Lett. **89**, 1 (2002).
[4] J. Birn, A. V. Artemyev, D.N. Baker, M. Echim, M. Hoshino, and L.M. Zelenyi, Sp. Sci. Rev. **173**, 49 (2012).
[5] Q. Pan, M. Ashour-Abdalla, R.J. Walker, and M. El-Alaoui, J. Geophys. Res. Sp. Phys. **119**, 1060 (2014).
[6] R.P. Lin and H.S. Hudson, Sol. Phys. **17**, 412 (1971).
[7] S. Masuda, T. Kosugi, H. Hara, S. Tsuneta, and Y. Ogawara, Nature **371**, 495 (1994).
[8] W. Fox, M. Porkolab, J. Egedal, N. Katz, and A. Le, Phys. Plasmas **17**, 072303 (2010).
[9] I. Klimanov, A. Fasoli, and T.P. Goodman, Plasma Phys. Control. Fusion **49**, L1 (2007).
[10] P. V. Savrukhin, Phys. Rev. Lett. **86**, 3036 (2001).
[11] S. Von Goeler, J. Stevens, S. Bernabei, M. Bitter, T.K. Chu, P. Efthimion, N. Fisch, W. Hooke, K. Hill, J. Hosea, F. Jobes, C. Karney, J. Mervine, E. Meservey, R. Motley, P. Roney, S. Sesnic, K. Silber, and G. Taylor, Nucl. Fusion **25**, 1515 (1985).
[12] K. Yamasaki, S. Inoue, S. Kamio, T.G. Watanabe, T. Ushiki, X. Guo, T. Sugawara, K. Matsuyama, N. Kawakami, T. Yamada, M. Inomoto, and Y. Ono, Phys. Plasmas **22**, 101202 (2015).
[13] M. Yamada, J. Yoo, J. Jara-Almonte, H. Ji, R.M. Kulsrud, and C.E. Myers, Nat. Commun. **5**, 4774 (2014).
[14] X. Guo, M. Inomoto, T. Sugawara, K. Yamasaki, T. Ushiki, and Y. Ono, Phys. Plasmas **22**, 101201 (2015).
[15] T. Ushiki, M. Inomoto, and H. Koguchi, IEEJ Trans. Fundam. Mater. **134**, 493 (2015).
[16] A. Retin, R. Nakamura, A. Vaivads, Y. Khotyaintsev, T. Hayakawa, K. Tanaka, S. Kasahara, M. Fujimoto, I. Shinohara, J.P. Eastwood, M. Andre, W. Baumjohann, P.W. Daly, E.A. Kronberg, and N. Cornilleau-Wehrlin, J. Geophys. Res. Sp. Phys. **113**, 1 (2008).
[17] G. Fiksel, A.F. Almagri, B. Chapman, V. Mirnov, Y. Ren, J. Sarff, and P. Terry, Phys. Rev. Lett. **103**, 145002 (2009).
[18] R.M. Magee, D.J. Den Hartog, S.T.A. Kumar, A.F. Almagri, B.E. Chapman, G. Fiksel, V. V. Mirnov, E.D. Mezonlin, and J.B. Titus, Phys. Rev. Lett. **107**, 065005 (2011).
[19] R.N. Dexter, D.W. Kerst, T.W. Lovell, and S.C. Prager, Fusion Technol. **19**, 131 (1991).
[20] J. Sarff, A. Almagri, J. Anderson, D. Brower, D. Craig, B. Deng, D. Den Hartog, W. Ding, G. Fiksel, C. Forest, V. Mirnov, S. Prager, and V. Svidzinski, Proc. Magn. Plasma Galaxy Evol. 48 (2005).
[21] S.C. Prager, A.F. Almagri, S. Assadi, J.A. Beckstead, R.N. Dexter, D.J. Den Hartog, G. Chartas, S.A. Hokin, T.W. Lovell, T.D. Rempel, J.S. Sarff, W. Shen, C.W. Spragins, and J.C. Sprott, Phys. Fluids B **2**, 1367 (1990).
[22] T.M. Biewer, C.B. Forest, J.K. Anderson, G. Fiksel, B. Hudson, S.C. Prager, J.S. Sarff, J.C. Wright, D.L. Brower, W.X. Ding, and S.D. Terry, Phys. Rev. Lett. **91**, 045004 (2003).
[23] J.A. Reusch, J.K. Anderson, D.J. Den Hartog, F. Ebrahimi, D.D. Schnack, H.D. Stephens, and C.B. Forest, Phys. Rev. Lett. **107**, 1 (2011).
[24] R.M. Magee, Ion Energization during Tearing Mode Magnetic Reconnection in a High Temperature Plasma, University of Wisconsin-Madison, 2011.
[25] A.M. DuBois, J.D. Lee, and A.F. Almagri, Rev. Sci. Instrum. **86**, 073512 (2015).
[26] J. Stevens, S. Von Goeler, S. Bernabei, M. Bitter, T.K. Chu, P. Efthimion, N.J. Fisch, W. Hooke, J. Hosea, F. Jobes, C. Karney, E. Meservey, R. Motley, G. Taylor, Nucl. Fusion **25**, 1529 (1985).
[27] R.W. Harvey and M.G. McCoy, Adv. Simul. Model. Thermonucl. Plasmas 498 (1992).
[28] H. Dreicer, Phys. Rev. **115**, 238 (1959).
[29] J.K. Anderson, J. Adney, A. Almagri, A. Blair, D.L. Brower, M. Cengher, B.E. Chapman, S. Choi, D. Craig, D.R. Demers, D.J. Den Hartog, B. Deng, W.X. Ding, F. Ebrahimi, D. Ennis, G. Fiksel, C.B. Forest, P. Franz, J. Goetz, R.W. Harvey, D. Holly, B. Hudson, M. Kaufman, T. Lovell, L. Marrelli, P. Martin, K. McCollam, V. V. Mirnov, P. Nonn, R. O'Connell, S. Oliva, P. Piovesan, S.C. Prager, I. Predebon, J.S. Sarff, G. Spizzo, V. Svidzinski, M. Thomas, and M.D. Wyman, Phys. Plasmas **12**, 1 (2005).
[30] R. O'Connell, D.J. Den Hartog, C.B. Forest, J.K. Anderson, T.M. Biewer, B.E. Chapman, D. Craig, G. Fiksel, S.C. Prager, J.S. Sarff, S.D. Terry, and R.W. Harvey, Phys. Rev. Lett. **91**, 045002 (2003).

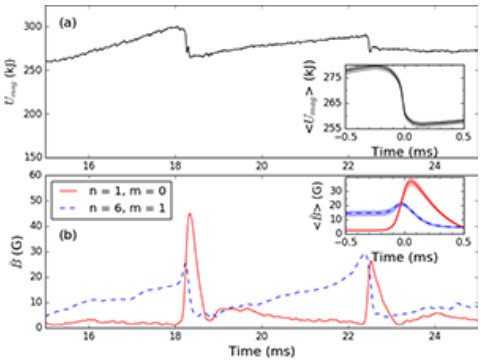

FIG. 1. (a) Evolution of U_{mag} for two magnetic relaxation cycles in a 500kA standard plasma in MST. (b) Evolution of tearing mode amplitudes for the edge-resonant m=0, n=1 (red, solid) mode and the (innermost) core-resonant m=1, n=6 (blue, dashed) mode. The insets show the magnetic energy (top) and tearing mode amplitudes (bottom) averaged over 485 events (shaded region represents the standard error of the mean), with time relative to MR.

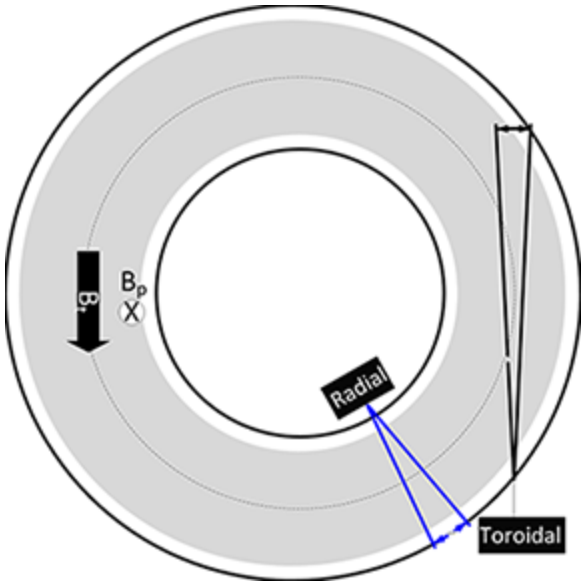

FIG. 2. A schematic of the FXR detector views.

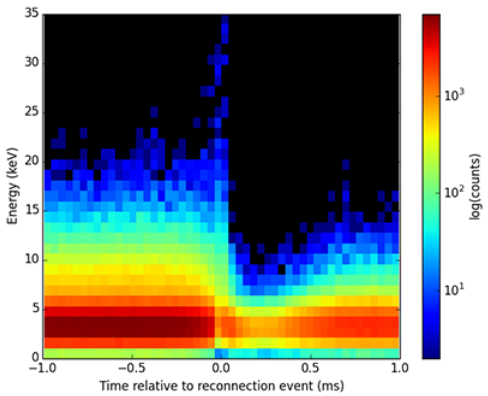

FIG. 3. The evolution of x-ray energy relative to MR (0ms), with colors indicating x-ray flux. Black indicates no flux and dark red indicates high flux.

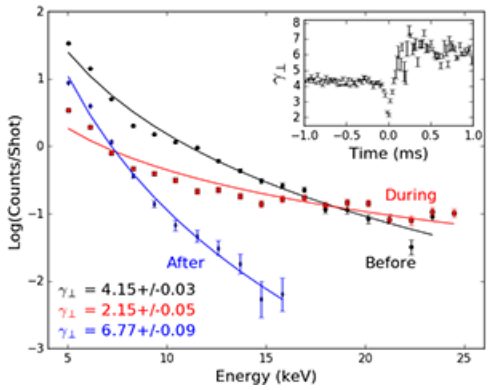

FIG. 4. X-ray spectra measured in the radial view for 20μs windows 0.5ms before (black), during (red) and 0.5ms after (blue) MR. Each spectrum is fit with a power-law (solid lines), from which $\gamma_\perp$ is calculated. The inset shows $\gamma_\perp$ as a function of time relative to MR.

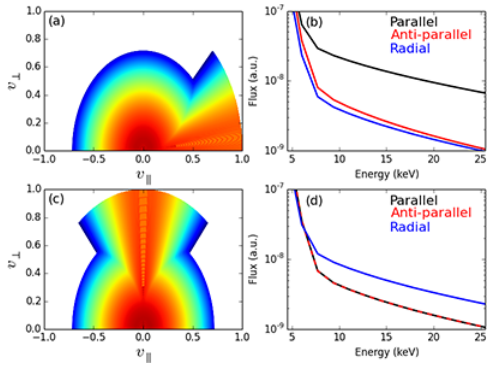

FIG. 5. (a) EDF used in CQL3D to model parallel anisotropy for a power-law tail distribution in $v_\parallel$. (b) Modeled bremsstrahlung x-ray emission for toroidal parallel (black), toroidal anti-parallel (red), and radial (blue) pencil-like lines-of-sight. (c) EDF used in CQL3D to model perpendicular anisotropy for a power-law tail distribution localized in $v_\perp$. (d) Modeled bremsstrahlung x-ray emission for the same lines-of-sight as in (b). For both cases, the tail is Gaussian and $v_\parallel$ and $v_\perp$ are normalized to $v_{norm} = 1.9\times10^8 m/s$. The modeled emission is normalized for volume of viewing cones through the plasma core.

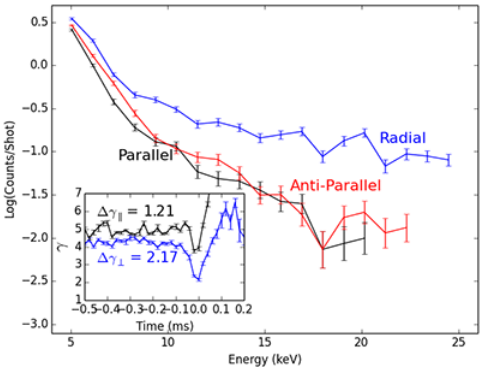

FIG. 6. X-ray spectra measured for parallel (black), anti-parallel (red) and radial (blue) views during a 20μs window during MR. The inset shows the evolution of γ for the parallel (black) and radial (blue) views.